Fracture of porous materials – Influence of the pore size

Dominique Leguillon, Romana Piat

Fracture of porous materials – Influence of the pore size

D. Leguillon[a,*], R. Piat[b]

[a] LMM – CNRS UMR 7607, University P. et M. Curie (Paris 6), Paris, France
[b] Institute of Solid Mechanics, University of Karlsruhe, Karlsruhe, Germany

The random distribution of pores in location, size and shape makes the fracture of porous materials a difficult problem. We address herein a simplified model of porous material as can be obtained for instance in ceramics by introducing organic or polymer particles prior to the sintering step. Resulting spherical pores are almost regularly located with a homogeneous distribution in size. A fracture criterion involving both toughness and tensile strength allows studying the competition between, on the one hand the crack blunting due to the pores and resulting in an apparent toughness enhancement, and on the other hand the weakening effect caused by an increasing volume fraction of pores.

Keywords: Porous materials; Fracture mechanics; Toughening; Weakening

1. Introduction

The random distribution of pores in location, size and shape makes the fracture of porous materials a difficult problem and a quite sparse literature exists in the domain. Contradictory results are often reported in fracture of porous materials: strengthening and weakening [1–6].

We address herein a simplified model of porous material as can be obtained for instance in ceramics by introducing organic or polymer particles like corn starch or polyamide prior to the sintering step. Resulting spherical pores are almost regularly located with a homogeneous distribution in size. Assuming the pores are small compared to the structure, a fracture criterion involving both toughness and tensile strength allows studying the competition between, on the one hand the crack blunting due to the pores and resulting in an apparent toughness enhancement; and on the other hand the weakening effect caused by an increasing volume fraction of pores.

* Corresponding author. LMM, University Paris 6, Case 162, 4 Place Jussieu, 75252 Paris cedex 05, France. Tel.: +33 144 275 322; fax: +33 144 275 259.
E-mail address: dol@ccr.jussieu.fr (D. Leguillon).

Nomenclature

a, d	ligament width and pore diameter (m)
A, D	scaling coefficients (MPa^{-1})
e	specimen thickness (plane elasticity) (m)
E, C, ν	Young's modulus, stiffness matrix (MPa) and Poisson's ratio
G	energy release rate ($\mathrm{J\,m}^{-2}$)
$G_\mathrm{c}, G_\mathrm{d}, G_\mathrm{p}$	toughness, generic, of a dense, of a porous ceramic ($\mathrm{J\,m}^{-2}$)
F_i	Gauge functions of the inner expansion
k_I	mode I stress intensity factor ($\mathrm{MPa\,m}^{1/2}$)
$k_\mathrm{I}^\mathrm{c}, k_\mathrm{I}^{\mathrm{c\ app}}$	toughness and apparent toughness ($\mathrm{MPa\,m}^{1/2}$)
ℓ, ℓ_0	crack increment length (generic and at initiation) (m)
$\underline{n}$	unit normal vector
R	ratio of the apparent toughness to the actual toughness of the material
$\underline{U}^\mathrm{d}$	actual displacement field (m)
$\underline{U}^0$	leading term of the outer expansion, far field (m)
$\underline{u}^\mathrm{I}$	angular mode I shape function (MPa^{-1})
$\underline{V}^i$	terms of the inner expansions, near field (MPa^{-1})
x_1, x_2, r, θ	physical Cartesian and polar coordinates
y_1, y_2, ρ, θ	stretched dimensionless coordinates
δW_p	change in potential energy (J)
Γ^∞	artificial outer boundary in Ω^in
μ, μ_0, ζ	stretched crack lengths (generic and at initiation) and ligament width
Ω^in	stretched "inner" domain
Σ, D, F	primary crack, cavity and new crack increment boundaries in Ω^in
$\sigma(\underline{X})$	tension orthogonal to the failure direction associated with $\underline{X}$ (MPa)
$\hat{\sigma}(\underline{X})$	modified tension associated with $\underline{X}$ (MPa)
$\tilde{\sigma}(\underline{Y})$	tension orthogonal to the failure direction associated with $\underline{Y}$ in Ω^{in}
σ_c	tensile strength (MPa)
$\underline{\underline{\tilde{\sigma}}}(\underline{Y})$	stress tensor with components $\tilde{\sigma}_{11}(\underline{Y}), \tilde{\sigma}_{12}(\underline{Y}), \tilde{\sigma}_{22}(\underline{Y})$ associated with $\underline{Y}$ in Ω^in
Ψ	path independent integral
∇_x, ∇_y, ∇_x^S, ∇_y^S	gradient and symmetric part of it with respect to x (resp. to y)

In a first step, the blunting effect due to a single pore is examined, the so-called key-hole problem [7]. It exhibits a strong size effect related to the pore diameter, larger the pore, higher the apparent toughness. This effect is due to the size of the pore whatever the size of the specimen (see also [8]), in this sense it differs from the statistical size effects analysed by Weibull [9] in a pioneering work. Nevertheless, in both cases homothetic specimens would lead to different results, either because of the size of the pore or the size of the specimen, and, based on experiments, it would be difficult to distinguish between the two approaches.

In Section 2, the effect of two neighbouring pores ahead of the primary crack is analysed. There is now a competition between the pore size effect leading to an apparent toughness enhancement and a weakening effect caused by the decreasing width of the ligament between pores. The section concludes on a brief analysis of the role of the shape of the pores considering circular and elliptical pores.

Next the role of collateral pores is analysed, the question being: under a symmetrical loading, does a crack can kink out of the symmetry axis toward the nearest pore?

Section 6 is dedicated to an attempt to generalize these results to porous materials. The selected model is quite simple; the system of pores is embedded in a neighbouring area of dense material, itself immersed in a homogeneous material with homogenized properties taking into account the volume fraction of pores.

2. Crack blunting by a cavity

2.1. The key-hole problem

Within the plane strain elasticity framework, we consider a cracked specimen (a CT specimen for instance, Fig. 1) in which the primary crack ends in a circular cavity of diameter d, small compared to any dimension of the structure and especially to the crack length.

The so-called "key-hole" problem consists in the prediction of the apparent toughness enhancement deriving from the blunting effect of the circular hole.

The solution $\underline{U}^{\mathrm{d}}$ to the elastic problem is expressed as the solution $\underline{U}^{0}$ to the unperturbed problem (i.e. the hole is not visible $d \to 0$) plus a correction, the smaller the pore diameter, the smaller the correction

$$\underline{U}^{\mathrm{d}}(x_1, x_2) = \underline{U}^{0}(x_1, x_2) + \text{small correction}. \tag{1}$$

The leading term $\underline{U}^{0}$ is the far field; it is a satisfying approximation of the actual solution $\underline{U}^{\mathrm{d}}$ except in the vicinity of the perturbation (i.e. the cavity at the crack tip). Note that there is an uncertainty of the order of d on the exact location of the crack tip in the unperturbed domain since details smaller or similar to d are not visible.

The near field brings complementary information. The space variables are dilated by $1/d$ and the limit $d \to 0$ is considered again. The resulting domain Ω^{in} is unbounded with a semi-infinite crack ending in a cavity with a unit diameter (Fig. 2).

The elastic solution expands in terms of the small parameter d and the stretched variables $y_i = x_i/d$ to form the inner expansion

$$\underline{U}^{\mathrm{d}}(x_1, x_2) = \underline{U}^{\mathrm{d}}(dy_1, dy_2) = F_0(d)\underline{V}^{0}(y_1, y_2) + F_1(d)\underline{V}^{1}(y_1, y_2) + \cdots \text{ with } \lim_{d \to 0} \frac{F_1(d)}{F_0(d)} = 0. \tag{2}$$

Taking into account the change of variables and the derivation rule $\nabla_y = 1/d\nabla_x$ (where ∇_x and ∇_y denote the gradient operators with respect to the physical space variables x_i and to the dimensionless variables y_i), an identification process in the elastic equations allows writing a set of equations in the variables y_i for each $\underline{V}^{i}$

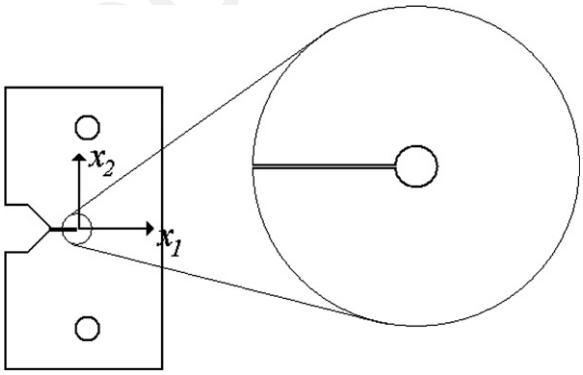

Fig. 1. The CT specimen and the "key-hole" termination of the primary crack.

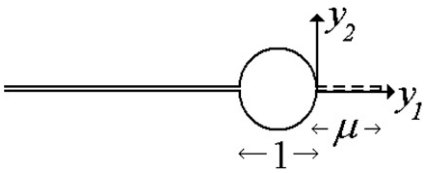

Fig. 2. The stretched single pore and the expected crack path.

$$\begin{cases} -\nabla_y \cdot \underline{\underline{\tilde{\sigma}}}(\underline{V}^{\mathrm{i}}) & = 0 & \text{in } \Omega^{\mathrm{in}}, \\ \underline{\underline{\tilde{\sigma}}}(\underline{V}^{\mathrm{i}}) & = C : \nabla_y^{\mathrm{S}} \underline{V}^{\mathrm{i}} & \text{in } \Omega^{\mathrm{in}}, \\ \underline{\underline{\tilde{\sigma}}}(\underline{V}^{\mathrm{i}}) \cdot \underline{n} & = 0 & \text{along } \Sigma \text{ and } D. \end{cases} \tag{3}$$

The first equation is the balance of momentum. The second one is the elastic constitutive law, C is the stiffness matrix and ∇_y^{S} the symmetric part of the gradient operator ∇_y. The last equation expresses stress free boundary conditions, Σ and D denote the primary crack faces and the boundary of the cavity, respectively.

This set of equations lacks of a statement prescribing the behaviour at infinity. The matching conditions between the outer and inner expansions will provide this additional relation [10]. The behaviour of the far field (unperturbed) near the crack tip (in the outer domain) writes

$$\underline{U}^0(x_1, x_2) = \underline{U}^0(0,0) + k_{\mathrm{I}} \sqrt{r} \underline{u}^{\mathrm{I}}(\theta) + \cdots \tag{4}$$

Where r and θ are the polar coordinates with the origin at the crack tip. The coefficient k_{I} is the mode I stress intensity factor of the classical square root behaviour of the opening mode I. The prescribed loading is supposed symmetric to avoid the antisymmetric mode II. The first term of the expansion is an irrelevant constant used for consistency. These terms must match with the leading terms of the inner expansion (2). Thus

$$F_0(d) = 1; \quad F_1(d) = k_{\mathrm{I}} \sqrt{d}; \quad \underline{V}^0(y_1, y_2) \approx \underline{U}^0(0,0) \quad \text{and} \quad \underline{V}^1(y_1, y_2) \approx \sqrt{\rho} \underline{u}^{\mathrm{I}}(\theta) \text{ with } \quad \rho = r/d, \tag{5}$$

where $\approx$ means "behaves like at infinity" (i.e. as $\rho \to \infty$). The problem in the unknown function $\underline{V}^0$ has a trivial solution

$$\underline{V}^0(y_1, y_2) = \underline{U}^0(0,0), \tag{6}$$

whereas $\underline{V}^1$ must be numerically computed by finite elements (FE) in an artificially bounded (at a large distance of the perturbation) domain with either a Neumann or a Dirichlet condition prescribed along the new artificial boundary Γ^{∞}

$$\underline{V}^1(y_1, y_2) = \sqrt{\rho} \underline{u}^{\mathrm{I}}(\theta) \text{ (Dirichlet)} \quad \text{or} \quad \underline{\underline{\tilde{\sigma}}}(\underline{V}^1) \cdot \underline{n} = \underline{\underline{\tilde{\sigma}}}(\sqrt{\rho} \underline{u}^{\mathrm{I}}(\theta)) \cdot \underline{n} \text{ (Neumann)}. \tag{7}$$

Finally the inner expansion writes

$$\underline{U}^{\mathrm{d}}(x_1, x_2) = \underline{U}^{\mathrm{d}}(dy_1, dy_2) = \underline{U}^0(0,0) + k_{\mathrm{I}} \sqrt{d} \underline{V}^1(y_1, y_2) + \cdots, \tag{8}$$

where $\underline{V}^1$ is solution of the complete set of Eqs. (3) and (7).

2.2. The onset of a new crack and the fracture criterion

Let us consider now a short crack with length ℓ facing the primary one (Fig. 2). The length is supposed to be smaller or of the same order of magnitude than d. As a consequence, the outer expansion (1) is unchanged since the details of the perturbation are not visible. The inner terms $\underline{V}^i$ are now solution to problems settled on an unbounded domain embedding a crack with dimensionless length $\mu = \ell/d$ (Fig. 2). The stress free boundary condition $(3)_3$ extends to the two faces F of the new crack. By analogy with (8), the corresponding inner expansion writes

$$\underline{U}^{\mathrm{d}}(x_1, x_2, \ell) = \underline{U}^{\mathrm{d}}(dy_1, dy_2, \mu d) = \underline{U}^0(0,0) + k_{\mathrm{I}} \sqrt{d} \underline{V}^1(y_1, y_2, \mu) + \cdots \tag{9}$$

The method follows that presented in [11], two conditions must be fulfilled, one involves the energy, the other the stress field. But it differs slightly since there are now two small parameters instead of one, and the stretching is performed with respect to d, not to ℓ as in [11]. Moreover, even if there is a stress concentration, the blunting due to the pore avoids any singularity. Thus, the stress field is derived from a FE computation instead of an explicit expression coming from the asymptotics as in [11]. The method is closer to that employed in [12,13].

The change in potential energy caused by the onset of the new crack expands as

$$-\delta W_{\mathrm{p}} = k_{\mathrm{I}}^2 d(A(\mu) - A(0)) e + \cdots = k_{\mathrm{I}}^2 \ell \frac{A(\mu) - A(0)}{\mu} e + \cdots, \tag{10}$$

where e holds for the specimen thickness (plane elasticity). The coefficient $A(\mu)$ is extracted from $\underline{V}^1$ using the path independent integral Ψ [10,14]

$$A(\mu) = \Psi\big(\underline{V}^1(y_1, y_2, \mu), \sqrt{\rho}\underline{u}^{\mathrm{I}}(\theta)\big) = \frac{1}{2}\int_{\Gamma}\Big[\underline{\tilde{\underline{\sigma}}}(\underline{V}^1)\cdot\underline{n}\cdot\sqrt{\rho}\underline{u}^{\mathrm{I}}(\theta) - \underline{\tilde{\underline{\sigma}}}(\sqrt{\rho}\underline{u}^{\mathrm{I}}(\theta))\cdot\underline{n}\cdot\underline{V}^1\Big]\mathrm{d}s, \tag{11}$$

where Γ is any contour in the inner domain with normal $\underline{n}$, surrounding the cavity and the crack extension and starting and finishing on the stress free faces Σ of the primary crack (see (13) below for the definition of $\underline{\tilde{\underline{\sigma}}}$).

The energy condition for fracture derives from an energy balance and reads [11,12]

$$-\delta W_{\mathrm{p}} \geqslant G_{\mathrm{c}} e\ell \Rightarrow G = -\frac{\delta W_{\mathrm{p}}}{e\ell} = k_{\mathrm{I}}^2\frac{A(\mu) - A(0)}{\mu} \geqslant G_{\mathrm{c}}. \tag{12}$$

Here G_{c} denotes the toughness of the material and $G_{\mathrm{c}}e\ell$ is the energy consumed to create a new crack surface $e\ell$.

Prior to the onset, in agreement with the well known Inglis solution [15], the inner expansion allows writing the tension along the axis facing the primary crack as

$$\underline{\underline{\sigma}}(\underline{U}^{\mathrm{d}}(x_1, 0)) = C : \nabla_x^{\mathrm{S}}\underline{U}^{\mathrm{d}}(x_1, 0) = \frac{1}{d}C : \nabla_y^{\mathrm{S}}\underline{U}^{\mathrm{d}}(\mathrm{d}y_1, 0, 0) = \frac{k_{\mathrm{I}}}{\sqrt{d}}\underline{\tilde{\underline{\sigma}}}(\underline{V}^1(y_1, 0, 0)) + \cdots \tag{13}$$

The function $(A(\mu) - A(0))/\mu$ involved in (12) is an increasing function of μ and thus (12) gives a lower bound for the admissible μ for a fixed intensity of the loading, i.e. for a fixed value of k_{I}.

On the other hand, $\underline{\tilde{\underline{\sigma}}}(y_1, 0)$ is a decreasing function of y_1. Fulfilling the traction condition $\sigma \geqslant \sigma_{\mathrm{c}}$ all along the expected crack path $0 \leqslant y_1 \leqslant \mu$ leads to (σ is the tension acting on the expected crack path and σ_{c} the tensile strength)

$$\frac{k_{\mathrm{I}}}{\sqrt{d}}\tilde{\sigma}(\underline{V}^1(\mu, 0, 0)) \geqslant \sigma_{\mathrm{c}}, \tag{14}$$

where $\tilde{\sigma}$ is the counterpart to σ in Ω^{in}. The inequality (14) provides an upper bound for the admissible μ. The fracture criterion proposed in [11] states that both the energy condition (12) and the stress condition (14) must be fulfilled at crack initiation. The compatibility of the two inequalities (12) and (14) (i.e. coincidence of the upper and lower bounds) leads to an equation for the dimensionless initiation length μ_0 that turns to be a function of d

$$\frac{1}{\tilde{\sigma}(\underline{V}^1(\mu_0, 0, 0))^2}\frac{A(\mu_0) - A(0)}{\mu_0} = \frac{1}{d}\frac{G_{\mathrm{c}}}{\sigma_{\mathrm{c}}^2}. \tag{15}$$

Finally the so-called apparent toughness can be derived from (12) and (15)

$$k_{\mathrm{I}}^{\mathrm{c\ app}} = \sqrt{\frac{G_{\mathrm{c}}}{D(d)}} \text{ with } D(d) = \frac{A(\mu_0) - A(0)}{\mu_0} \quad \text{and} \quad \mu_0 = \mu_0(d) \quad \text{according to (15)}. \tag{16}$$

This toughness is baptised apparent to recall that in any case the cavity is small compared to the whole structure or specimen and that the only visible mechanism is a crack growth a priori governed by the Griffith (or Irwin, see below) criterion.

The Irwin formula (E and ν hold for the Young's modulus and Poisson's ratio of the material)

$$G_{\mathrm{c}} = \frac{1 - \nu^2}{E}k_{\mathrm{I}}^{\mathrm{c}}, \tag{17}$$

leads to derive the relative apparent toughness which is a meaningful parameter assessing the toughening/weakening effect

$$R = \frac{k_{\mathrm{I}}^{\mathrm{c\ app}}}{k_{\mathrm{I}}^{\mathrm{c}}} = \sqrt{\frac{1 - \nu^2}{ED(d)}}. \tag{18}$$

Here $R > 1$ (resp. $R < 1$) holds for a toughening (resp. weakening) effect.

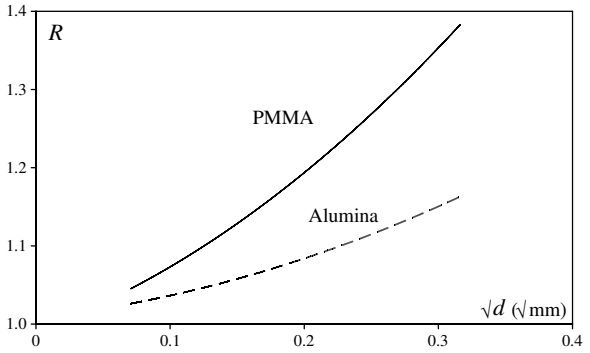

Fig. 3. The relative apparent toughness $R = k_I^{c\ app}/k_I^c$ vs. the square root of the cavity diameter d ($mm^{1/2}$).

Table 1
Critical distance ℓ_0 as a function of the pore diameter d

d (μm)	10	20	30	40	50	60	70	80	90	100
PMMA ℓ_0 (μm)	13	15	17	18	19	20	21	22	23	24
Alumina ℓ_0 (μm)	37	39	42	44	46	48	50	51	53	54

The presence of d in (15), (16) and (18) shows that there is a size effect which is due to the actual diameter of the pore not to any dimensionless ratio.

Fig. 3 plots the ratio R (18) as a function of d for two different materials: a polymer (PMMA: $E = 2.3$ GPa, $v = 0.3$, $G_c = 394$ J m^{-2}, $\sigma_c = 124$ MPa) and a ceramic (Alumina: $E = 350$ GPa, $v = 0.3$, $G_c = 45.4$ J m^{-2}, $\sigma_c = 290$ MPa). Since there is a single material, FE computations can be carried out once for all with a dimensionless Young's modulus $E = 1$. Then, appropriate changes in the values of G_c and σ_c must be brought to carry out the fracture criterion in the two materials. The Poisson's ratio is taken 0.3 in both cases (anyway it plays a minor role within a reasonable range [16]).

Not surprisingly, this model does not exhibit a threshold below which the toughness enhancement is not visible as often invoked in the experimental results. Indeed this threshold is probably a consequence of the microstructure of the material (grain size for instance in ceramics) that is not addressed here. The materials are only described by macroscopic parameters like Young's modulus, toughness... However, there is a continuous trend in Fig. 3 and it is clear that below $d = 0.01$ mm the predicted gain in toughness is lower than 5%, and thus probably below the available accuracy of the measures.

In this criterion the fracture length $\ell_0 = \mu_0 d$ plays an important role. In a sense, it is not so far from the Theory of the Critical Distance (TCD) involved in [17,18], the aim of the present special issue. Herein, due to a decreasing function of the distance, the stress condition for failure can be interpreted as follows: prior to crack initiation, the tension σ at the distance ℓ_0 of the cavity must fulfil $\sigma = \sigma_c$ (see (13) and (14)); just like in the TCD or in the point stress criterion [19]. But it differs because ℓ_0 cannot be considered as a material parameter. As emphasized in Eq. (15) and illustrated in Table 1, it is a function of the cavity diameter d.

The critical length ℓ_0 does not vary strongly. It increases by a factor 1.8 and 1.5 for PMMA and Alumina, respectively, while d increases by 10. Nevertheless, it cannot be considered as a constant otherwise the size effect (16) would disappear.

3. Competition between strengthening and weakening in case of two cavities

3.1. The revised criterion for two circular cavities

In Section 2 it has been shown that a single pore at the tip of a crack increases the apparent toughness, larger the pore, larger the enhancement. In porous materials other pores are located ahead of the crack tip. In order to study their influence, in a first step we consider a simplified system made of two pores. A new

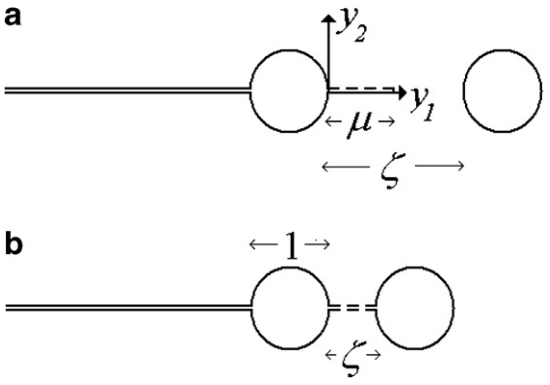

Fig. 4. The two pores and the expected crack path (in the stretched domain), (a) mix criterion when $\mu < \zeta$, (b) energy criterion when $\mu > \zeta$.

parameter intervenes: the ligament width a between the two pores or more precisely its dimensionless form $\zeta = a/d$, the ratio of the actual ligament width to the pore diameter (Fig. 4).

Provided the ligament width is smaller or of the same order of magnitude than the pore diameter, the far field is once again unchanged, details are not visible at the macro-scale. On the other hand, the stretched inner domain now embeds two pores with a unit diameter, the ligament width in between is ζ and it is partially or totally cut by a crack starting from the first pore toward the second one with dimensionless length $\mu \leqslant \zeta$. The inner expansion keeps the same form (8), the stress free boundary conditions in (3) extending to the second cavity. The function $\underline{V}^1$ and the coefficient A now depend on the two parameters μ and ζ. The inner expansion writes

$$\underline{U}^{\mathrm{d}}(x_1, x_2, \ell, a) = \underline{U}^{\mathrm{d}}(dy_1, dy_2, \mu d, \zeta d) = \underline{U}^0(0,0) + k_{\mathrm{I}}\sqrt{d}\,\underline{V}^1(y_1, y_2, \mu, \zeta) + \cdots \tag{19}$$

The coefficient A involved in the energy release rate still derives from the contour integral Ψ mentioned in (11)

$$A(\mu,\zeta) = \Psi\big(\underline{V}^1(y_1, y_2, \mu, \zeta), \sqrt{\rho}\underline{u}^{\mathrm{I}}(\theta)\big) = \frac{1}{2}\int_{\Gamma}\Big[\underline{\tilde{\sigma}}(\underline{V}^1)\cdot\underline{n}\cdot\sqrt{\rho}\underline{u}^{\mathrm{I}}(\theta) - \underline{\tilde{\sigma}}(\sqrt{\rho}\underline{u}^{\mathrm{I}}(\theta))\cdot\underline{n}\cdot\underline{V}^1\Big]\mathrm{d}s. \tag{20}$$

By analogy, the notations in this section are similar to that of Section 2; nevertheless, they correspond to different constants and functions since the geometry of the problem is changed.

The energy balance writes

$$G = -\frac{\delta W_{\mathrm{p}}}{e\ell} = k_{\mathrm{I}}^2\frac{A(\mu,\zeta) - A(0,\zeta)}{\mu} \geqslant G_{\mathrm{c}}. \tag{21}$$

For a fixed value of ζ and a prescribed loading (occurring in (21) through k_{I}), the left hand side member is still an increasing function of μ leading to a lower bound for the admissible lengths μ. But the tension $\tilde{\sigma}(\underline{V}^1(y_1, 0, 0, \zeta))$ acting on the ligament prior to any crack onset (see (13)) is no longer a decreasing function of the distance to the first pore (Fig. 5). It is first decreasing and then it increases again when approaching the second pore, there is a stress concentration in the vicinity of each pore but stronger near the first one. Then $\tilde{\sigma}$ must be replaced by the function:

$$\hat{\sigma}(y_1,\zeta) = \operatorname*{Inf}_{0\leqslant s\leqslant y_1}, \tilde{\sigma}(\underline{V}^1(s,0,0,\zeta)), \tag{22}$$

such that the condition ensuring the tension to be larger than the strength σ_{c} all along the putative crack path $0 \leqslant y_1 \leqslant \mu$ writes

$$\frac{k_{\mathrm{I}}}{\sqrt{d}}\hat{\sigma}(\mu,\zeta) \geqslant \sigma_{\mathrm{c}}. \tag{23}$$

The compatibility between (21) and (23) finally takes the form

$$\frac{1}{\hat{\sigma}(\mu_0,\zeta)^2}\frac{A(\mu_0,\zeta) - A(0,\zeta)}{\mu_0} = \frac{1}{d}\frac{G_{\mathrm{c}}}{\sigma_{\mathrm{c}}^2}. \tag{24}$$

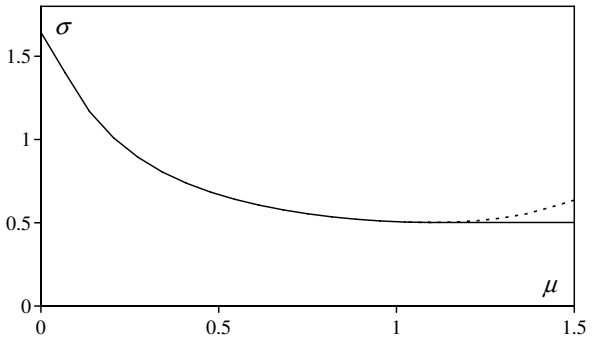

Fig. 5. The tension $\tilde{\sigma}$ acting on the ligament (dotted line) and the modified function $\hat{\sigma}$ (solid line) for $\zeta = 1.5$.

The apparent toughness is now a function of both d and a

$$k_{\mathrm{I}}^{\mathrm{c\ app}} = \sqrt{\frac{G_{\mathrm{c}}}{D(d,a)}} \quad \text{and} \quad R = \frac{k_{\mathrm{I}}^{\mathrm{c\ app}}}{k_{\mathrm{I}}^{\mathrm{c}}} = \sqrt{\frac{1-\nu^2}{ED(d,a)}}, \tag{25}$$

with $D(d,a) = \dfrac{A(\mu_0,\zeta) - A(0,\zeta)}{\mu_0}$; $\mu_0 = \mu_0(d,\zeta)$ according to (24) and $\zeta = a/d$.

Figs. 6 and 7 exhibit the competition between weakening and strengthening effects in two different materials: PMMA and Alumina. The strengthening is due to the crack blunting whereas the weakening is caused by the proximity of the second pore. The lack of smoothness (arrows in Figs. 6 and 7) is a consequence of two regimes. If the distance between pores is small, the initiation length μ_0 is larger than the ligament width ζ, then the crack jumps from one pore to the next one and this mechanism is uniquely governed by the energy condition, the stress condition is trivially satisfied. It leads to a weakening effect. Whereas if the distance between pores is large, there is first a crack initiation governed by the condition

$$k_{\mathrm{I}} \geqslant k_{\mathrm{I}}^{\mathrm{c\ app}}, \tag{26}$$

followed by a crack growth toward the next pore. It occurs when the initiation length μ_0 is much smaller than the ligament width ζ. Then the situation is close to the previous one (a single pore), the crack can jump the initiation length without a strong influence of the next pore, there is a strengthening effect.

Note that the energy criterion alone, based on the fracture of the whole ligament whatever its width, and always leads to a weakening since there is a smaller amount of matter to break due to the pores. It is plotted in

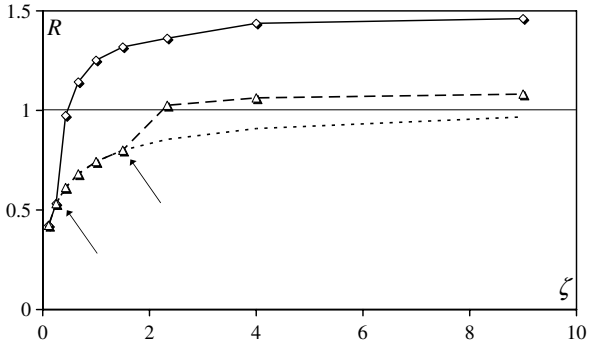

Fig. 6. The weakening/strengthening effects for $d = 0.1$ mm (solid line) and $d = 0.01$ mm (dashed line) in PMMA in function of the dimensionless distance between pores $\zeta = a/d$. The dotted line represents the energy criterion (for comparison). The arrows point toward the transition point between energy and mix criterion.

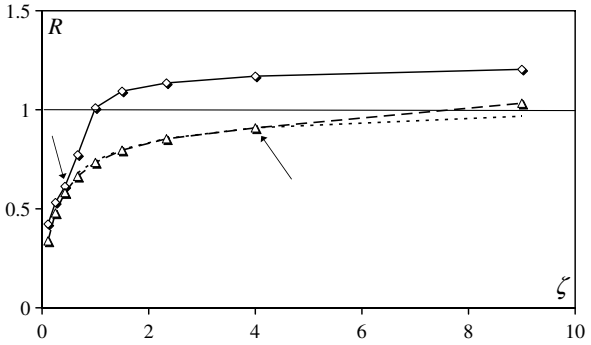

Fig. 7. The weakening/strengthening effects for $d = 0.1$ mm (solid line) and $d = 0.01$ mm (dashed line) in Alumina in function of the dimensionless distance between pores $\zeta = a/d$. The dotted line represents the energy criterion (for comparison) and almost confounds with the dashed line. The arrows point toward the transition point between energy and mix criterion.

Figs. 6, 7, 11, 13 and 14 for comparison (dotted line). Above the transition point (arrow) the energy criterion still holds true but is no longer a sufficient condition.

For $d = 0.1$ mm the strengthening effect due to the blunting is visible for $\zeta \geqslant 0.4$ (i.e. $a \geqslant 0.04$ mm) in PMMA and $\zeta \geqslant 1 (a \geqslant 0.1$ mm) in Alumina. This effect diminishes clearly for $d = 0.01$ mm, it remains but with a slight strengthening for $\zeta \geqslant 2 (a \geqslant 0.02$ mm) in PMMA and almost disappears in Alumina (it confounds with the energy criteria). Complementary computations have been carried out for smaller pores: $d = 0.001$ mm, but no toughness enhancement can be longer observed for the two materials in that case.

Some small discrepancies can be observed between Fig. 3 on the one hand, and 6 and 7 on the other hand, when ζ becomes large, thus when the influence of the second pore becomes negligible. They are perceptible mainly for $d = 0.1$ mm in PMMA when ℓ_0 becomes small compared to d (Table 1), i.e. μ_0 small compared to 1. They are due to FE inaccuracies; meshes differ in the two geometries (one or two pores) and should have been strongly refined near the inital pore when short crack increments are involved, to have an enough large number of broken elements. Nevertheless, the discrepancies do not exceed 5% in the worse case and are smaller ($\approx$1%) in the other ones.

3.2. The influence of the shape of the pores

The shape of the pores plays a role in the above phenomena but smaller than expected. Fig. 9 compares, in PMMA, circular pores to elliptical ones for which the ratio between the long and short axis equals three. They

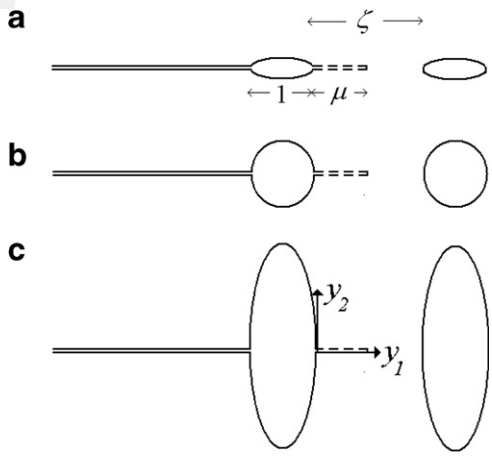

Fig. 8. The different tested pore shapes. The aspect ratio for ellipses is three. (a) horizontal elliptical pores, (b) circular pores, (c) vertical elliptical pores.

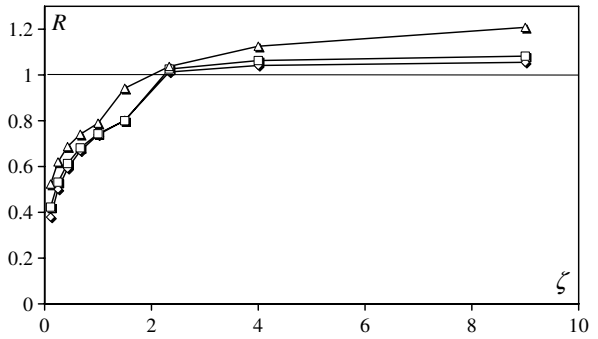

Fig. 9. The weakening/strengthening effects in PMMA for $d = 0.01$ mm for different pores shapes in function of the dimensionless distance between pores $\zeta = a/d$, vertical elliptical pores (triangles), circular pores (squares), horizontal elliptical pores (diamonds).

are horizontally (respectively vertically) placed along the crack axis (Fig. 8), in both cases the length of the horizontal axis of the ellipse is $d = 0.01$ mm (stretched to 1 in Fig. 8).

Vertical elliptical pores lead to a significant blunting effect while horizontals ones do not exhibit a contrary effect and roughly confound with the circular pores.

4. Crack deflection out of the symmetry axis

Under a symmetric loading, the question is: can a crack kink out of the straight symmetry axis to grow toward the nearest pore? To this purpose, we consider the following simplified frame made of four pores. The primary crack ends in the first pore, there are two symmetric pores aside of the symmetry axis and a fourth pore ahead, on the symmetry axis but at a larger distance than the two collateral ones (Fig. 10). Note that even if the structure is symmetric a random distribution of micro flaws (at a smaller scale than the pore diameter) induces a single (thus non symmetric) deflection rather than two symmetric ones as shown in Fig. 10.

Fig. 11 illustrates the competition between the two considered mechanisms: the straight propagation of the crack along the symmetry axis and the crack kinking toward the nearest collateral pore. Clearly the straight propagation is promoted except for collateral pores very close to the primary (blunted) crack tip.

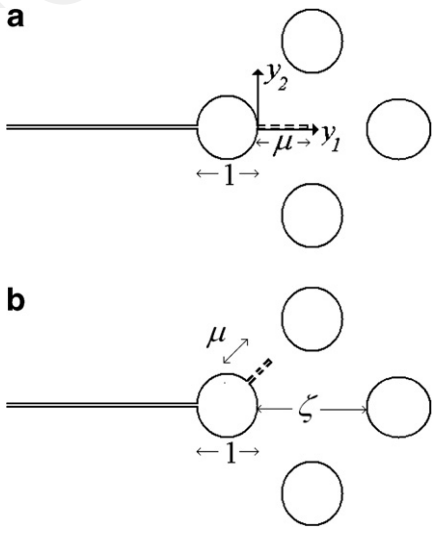

Fig. 10. The four pores system and the two expected crack paths (in the stretched domain), (a) straight propagation along the symmetry axis, (b) kink toward the nearest collateral pore.

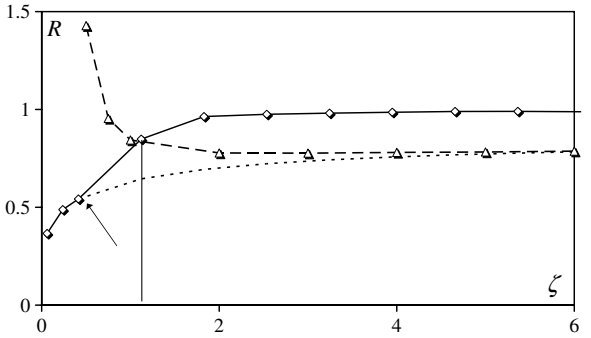

Fig. 11. The competition between the straight propagation along the symmetry axis (dashed line) and the crack kinking toward the nearest pore (solid line) in PMMA for $d = 0.01$ mm. For ζ below the marked line the crack kinks out of the symmetry axis. The dotted line represents the energy criterion for the kinked crack (for comparison). The arrow points toward the transition point between energy and mix criterion. For the straight propagation the mix criterion is solely involved.

The transition between deflection and straight propagation occurs for a dimensionless distance between pores ζ slightly larger than 1 and this value remains almost unchanged for other pore sizes (either smaller $d = 0.001$ mm or larger $d = 0.1$ mm) even if the mechanisms are different. For smaller values of d, the energy criterion is involved for both curves while it is the mix criterion that governs for larger d (see Fig. 11).

5. Crack growth in a porous material

Contradictory results are reported in the fracture behaviour of porous materials: strengthening and weakening just as in Section 3. Thus, an attempt is made in this section to generalize the above approach, that exhibits such a phenomenon, to the study of a crack growth in a porous material.

Nevertheless, even with a regular distribution of pores in size, shape and location, the above approach remains of a very high complexity. The dilatation $y_i = x_i/d$ leads to a set of infinitely many pores distributed in a dense matrix throughout the unbounded stretched domain and it is impossible to carry out any FE analysis. Strong simplifications are required. Only the two nearest pores ahead of the crack tip are kept, embedded in a neighbouring region made of dense material. This region is itself immersed in a homogeneous material (Fig. 12) with homogenized properties, which plays the role of the remote structure made of infinitely many pores in a dense matrix. This means that distant pores are assumed not to influence significantly the fracture process except through an average (homogenized) effect. The porosity V (the surface fraction of pores in plane elasticity) depends both on the pore diameter d and the distance between pores a

$$V = \frac{\pi}{4}\frac{1}{(\varsigma+1)^2} \text{ with } \varsigma = a/d. \tag{27}$$

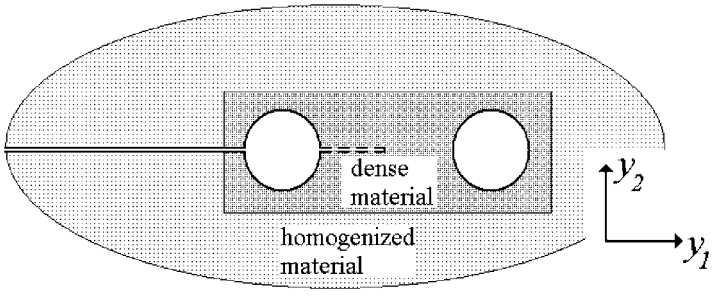

Fig. 12. The simplified model of porous material made of a neighbouring area of dense material embedded in the homogenized porous material.

The Poisson's ratio is kept unchanged. The homogenized Young's modulus E^{hom} is derived by a law of mixture taking into account the porosity V and vanishing at percolation of pores ($\zeta = 0$, $V = \pi/4 \simeq 0.78$)

$$E^{\text{hom}} = E\left(1 - \frac{4V}{\pi}\right). \tag{28}$$

It is a coarse approximation and, as will be seen further, the trends observed in the preceding sections are not strongly modified.

The energy criterion expressed in terms of k_{I}^{c} and $k_{\text{I}}^{\text{c app}}$ is independent of the Young's modulus as well as of the actual toughness of the dense material. It exhibits a "master curve" as already used in [12,16], it works in case of very small pores for PMMA or small to very small pores in Alumina. For larger pores, the mix criterion takes precedence and the strengthening effect is visible for small volume fraction of pores (Figs. 13 and 14).

The agreement between the predictions and the experiments is illustrated in Fig. 15 which shows a comparison of the present model with experimental results on two different ceramics: SiC and B_4C [4,6]. G_p/G_d is the dimensionless ratio of the (apparent) toughness of the porous material to the toughness of the dense ceramic. As expected, no reinforcement is observable. The prediction slightly underestimates the toughness for small porosities. Nevertheless, despite an outrageously simplified model there is a satisfying agreement.

In these tests, the porosity is obtained by adding spherical particles of polyamide, PTFE or corn starch during the sintering process (various symbols in Fig. 15), that are burned out at the end of the elaboration phase. It leads to a quite regularly distributed porosity made of spherical pores with $d \simeq 0.01$ mm.

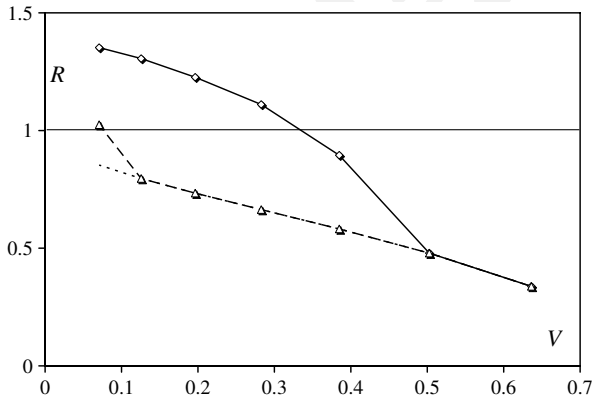

Fig. 13. Relative toughness of a porous PMMA in function of the of porosity. Energy criterion (dotted line) (for comparison), mix criterion (dashed line $d = 0.01$ mm, solid line $d = 0.1$ mm).

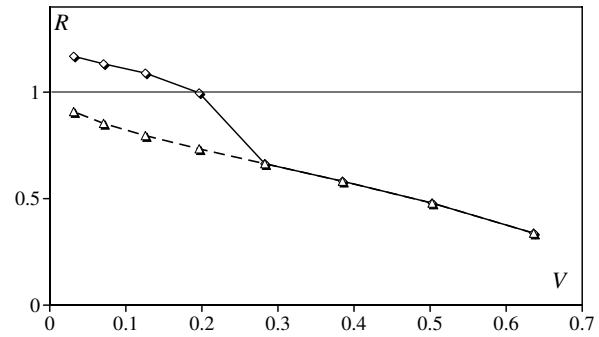

Fig. 14. Relative toughness of a porous Alumina in function of the porosity. The mix criterion (dashed line) confounds with the energy (dotted line, invisible) for small pores ($d = 0.01$ mm). The strengthening effect is visible only for larger pores (solid line, $d = 0.1$ mm).

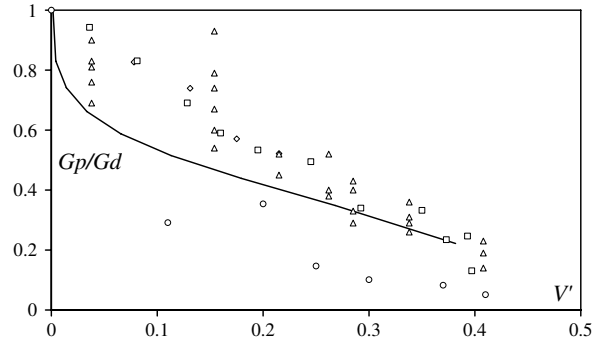

Fig. 15. Comparison between the predicted toughness (solid line) and experiments for two different ceramics: B_4C with corn starch particles (circles), SiC with corn starch particles (squares), SiC with polyamide particles (diamonds), SiC with PTFE particles (triangles).

To carry out the comparison more closely we have used the volume fraction of pores V' [6]

$$V' = \frac{\pi}{6}\frac{1}{(\varsigma+1)^3} \text{ with } \varsigma = a/d, \tag{29}$$

and as a consequence a law of mixture vanishing at percolation of pores (i.e. $\zeta = 0$, $V' = \pi/6 \simeq 0.52$). It is reported in [6] that the Young's modulus and the toughness of the porous ceramic vanish around this value.

In this section as above, it is assumed that the initial location of the primary crack tip is in a pore, leading to a tip blunting. It is a reasonable assumption provided there are enough pores to attract the crack, i.e. provided the pores are not too much distant from each other. For $V = 0.1$ the distance between pores is lower than twice the pore diameter ($\varsigma = 1.8$) if the surface fraction of pore is considered (27); it is even smaller if the volume fraction of pore (29) is used ($\zeta = 0.7$). On the other hand, it is illusory to consider the limit $V \to 0$ because in that case the crack should grow mainly within a dense material without meeting any pore and neither weakening nor toughening would be observed, leading to $R = 1$.

6. Conclusion

The model of porous material is outrageously simplified: it is a 2D model based on a very schematic geometry with homogenized material properties except in a very close vicinity of the primary (blunted) crack tip. Nevertheless, it leads to a satisfying and conservative agreement with experiments. The mix criterion involving both strength and toughness of the dense material is able to render the pore size effect leading to an apparent strengthening for relatively large pores ($d = 0.1$ mm) and low fractions of voids. This strengthening effect diminishes with the pore size, it almost disappear in alumina for $d = 0.01$ mm for instance whatever the volume fraction of pores.

Recent discussions have evidenced another scenario that is likely to occur in case of high porosity (i.e. small ligament widths): a jump of the crack toward and then through the next pore, leading to a new instantaneous initiation starting from the second pore. A very similar analysis can be carried out in this situation with simply a different crack extension (Fig. 4) and as a consequence new values of the coefficient $A(\mu)$. Small changes can be expected but only for very high porosities.

References

[1] Zimmermann A, Hoffman M, Flinn BD, Bordia RK, Chuang TJ, Fuller ER, et al. Fracture of alumina with controlled pores. J Am Ceram Soc 1998;81:2449–57.

[2] Deng ZY, She J, Inagaki Y, Yang JF, Ohji T, Tanaka Y. Reinforcement by crack-tip blunting in porous ceramics. J Eur Ceram Soc 2004;24:2055–9.

[3] Fujita H, Jefferson G, Mc Meeking RM, Zok FW. Mullite/alumina mixtures for use as porous matrices in oxide fiber composites. J Am Ceram Soc 2004;87(2):261–7.

[4] Tariolle S, Reynaud C, Thévenot F, Chartier T, Besson JL. Preparation and mechanical properties of SiC–SiC and B_4C–B_4C laminates. J Solid State Chem 2004;177:487–92.
[5] Reynaud C, Thévenot F, Chartier T, Besson JL. Mechanical properties and mechanical behaviour of SiC dense-porous laminates. J Eur Ceram Soc 2005;25:589–97.
[6] Leguillon D, Tariolle S, Martin E, Chartier T, Besson JL. Prediction of crack deflection in porous/dense ceramic laminates. J Eur Ceram Soc 2006;26:343–9.
[7] Smith E. Underpinning of a simple blunt flaw fracture initiation relation. Int J Fract 2005;131:401–15.
[8] Leguillon D, Quesada D, Putot C, Martin E. Prediction of crack initiation at blunt notches and cavities – size effects. Engng Fract Mech, doi:10.1016/j.engfracmech.2006.11.008.
[9] Weibull W. A statistical theory of the strength of materials. Proceedings of the Royal Swedish Academy of Engineering Science 1939;151:1–45.
[10] Leguillon D, Sanchez-Palencia E. Computation of singular solutions in elliptic problems and elasticity. New York: John Wiley& Son; 1987.
[11] Leguillon D. Strength or toughness? a criterion for crack onset at a notch. Eur J Mech A/Solids 2002;21:61–72.
[12] Leguillon D, Yosibash Z. Crack onset at a v-notch. Influence of the notch tip radius. Int J Fract 2003;122:1–21.
[13] Martin E, Leguillon D. Energetic conditions for interfacial failure in the vicinity of a matrix crack in brittle matrix composites. Int J Solids Struct 2004;41:6937–48.
[14] Labossiere PEW, Dunn ML. Stress intensities at interface corners in anisotropic bimaterials. Engng Fract Mech 1999;62:555–75.
[15] Timoshenko SP, Goodier JN. Theory of elasticity. 3rd ed. New York: Mc Graw Hill; 1970.
[16] Picard D, Leguillon D, Putot C. A method to estimate the influence of the notch-root radius on the fracture toughness of ceramics. J Eur Ceram Soc 2006;26:1421–7.
[17] Taylor D, Cornetti P, Pugno N. The fracture mechanics of finite crack extension. Engng Fract Mech 2005;72:1021–38.
[18] Taylor D. The theory of critical distances, in this special issue.
[19] Whitney JM, Nuismer RJ. Stress fracture criteria for laminated composites containing stress concentrations. J Comp Mater 1974;8:71–108.